Published in final edited form as:
Nucl Instrum Methods Phys Res A. 2013 January 21; 699: 205–210. doi:10.1016/j.nima.2012.04.029.

Development of a Head Scanner for Proton CT

H. F.-W. Sadrozinski[*], **R. P. Johnson**, **S. Macafee**, **A. Plumb**, **D. Steinberg**, and **A. Zatserklyaniy**
Santa Cruz Institute for Particle Physics, UC Santa Cruz, Santa Cruz, CA 95064, USA

V. Bashkirov, F. Hurley and **R. Schulte**
Loma Linda University Medical Center, Loma Linda, CA 92354, USA

Abstract

We describe a new head scanner developed for Proton Computed Tomography (pCT) in support of proton therapy treatment planning, aiming at reconstructing an accurate map of the stopping power (S.P.) in a phantom and, in the future, in patients. The system consists of two silicon telescopes which track the proton before and after the phantom/patient, and an energy detector which measures the residual energy or range of the proton to reconstruct the Water Equivalent Path Length (WEPL) in the phantom. Based on the experience of the existing prototype and extensive Geant4 simulations and CT reconstructions, the new pCT scanner will support clinically useful proton fluxes.

Keywords

Proton CT; Proton treatment planning; Head scanner; Silicon strip detector; Range counter; SiPM

1 INTRODUCTION

Proton therapy and treatment planning requires the knowledge of the stopping power (S.P.) in the patient, such that by tuning the proton energy, the Bragg peak can be located within the tumor. The goal of Proton CT (pCT) is to reconstruct a 3D map of the S.P. by measuring the residual range of protons of higher energy than those stopping in the patient. We presented the requirements for pCT in 2002 [1], and proposed in 2003 a detector system [2], which incorporated the basic building blocks of a pCT system: a tracker to measure the proton path before and after the phantom, and allows to calculate the Most Likely Path (MLP) the proton has taken within the phantom [3], and an energy detector to measure the residual energy or range of the proton, which is used to calculate the Water Equivalent Path Length (WEPL) in the phantom.

Since Multiple Coulomb Scattering (MCS) is a major issue to the spatial precision of the localization of the proton path, we confirmed in a beam test that the path inside a phantom can be predicted with sub-mm precision using external tracking and the MLP formalism [4]. We have constructed a prototype scanner based on detector technology developed in High Energy Physics (silicon strip sensors and CsI hodoscopic calorimeter) [5], and it is now used

[*]Corresponding author, hartmut@scipp.ucsc.edu, Tel: (831) 459 4670, Fax:(831) 459 5777.

to develop methods for calibrating the instrument in terms of WEPL and to refine image reconstruction methods [6]. In the following we describe a new pCT head scanner now under construction which will allow data taking at speeds required for clinical application, and which is expected to minimize the needs for detector calibration and data corrections. In Section 2 we present its design, layout and principle of operation, which are based on lessons learned from the existing detector and extensive Geant4 simulations. Section 3 has details of the research on the silicon tracking system, and Section 4 describes the on-going work on the energy detector.

2 DESIGN OF THE PCT HEAD SCANNER

The requirement that the MLP and the integrated S.P. be determined for every proton presents an instrumental challenge due to the large amount of data needed for pCT. To reconstruct the 3D S.P. map, 2D images are taken in a rotational scan with typical 2 degree steps (e.g. about the vertical axis in Fig. 1). For each of these 180 “views, one needs to have sufficient proton histories in each 1 mm^3 voxel to reliably determine the contribution of that voxel to the integrated S.P. The number of required protons has been estimated in Refs. [7] and [8], where the image quality was compared to the number of proton histories in the voxels. Stable solutions were found with 25 proton histories. Taking into account the loss of protons due to non-ionizing interactions in the phantom (~50%) and an additional loss of 50% in the fitting procedure for the most probable value in the residual energy, we find that we need 100 protons for every $1mm^3$ voxel in each of the 180 views, which requires ~ $7*10^8$ protons for a head-size object. With 10 kHz data rate, which is the data acquisition speed of our prototype scanner [5], one pCT scan will take 20 hrs, while a scan with a proton rate of 2 MHz will take 6 min. Our key specification is that proton histories can be acquired at a sustained 2 MHz rate to permit clinical application. Progress in data analysis might allow us to fit the entire residual energy spectrum instead of just the end-point, reducing the required number of proton histories, the needed scan time.

Figure 1 shows the layout of the head scanner. Protons with kinetic energy of 200 MeV coming from the left encounter the entrance telescope, the phantom, the exit telescope and are stopped in the energy detector/range counter. The entrance and exit telescopes each consist of two x-y planes of silicon sensors to allow the extrapolation of the proton trajectory into the phantom. The head phantom is mounted on a stage which can be rotated through a vertical axis. Not shown are the accelerator window and a scattering foil which enlarges the beam, about 200 cm upstream from the center of the phantom.

The desire to image a large volume of the head determines the lateral dimensions of the scanner. The aspect ratio is given by the goal to reconstruct a limited number of vertical “slices” of the 3D S.P. map, while the entire width of the head has to be covered in all “views”. The active area is 9 cm high and 36 cm wide, allowing the use of silicon sensors from 6” wafers as shown in Figs. 1 and 4.

An important design criterion for the scanner is compactness to reduce interferences within the gantry area. This means that all distances along the proton path should be minimized whenever possible. Using high-precision silicon sensors allows reducing the sensor separation D in the entrance and exit telescopes, (see Fig. 2), and is set to D = 5 cm, as discussed in more detail in Sec. 3.3. The distance L between entrance (front) and exit (back) telescope is a critical parameter, and has been investigated with GEANT4 simulations of a Herman head phantom [9], followed by reconstruction [6] of the relative stopping power (RSP), which is the S.P. relative to water.

In Fig. 3, we clearly see a difference in the reconstructed images from simulations with L=50 cm and 30 cm. To quantify the image quality, we introduce the reconstruction error σ_{Rec} as a measure of the goodness of the reconstruction:

$$\sigma_{\mathrm{Rec}} = \sqrt{\sum_{Voxels} \{RSP_i(reconstructed) - RSP_i(phantom)\}^2},$$

where we add in quadrature the RSP differences in the voxels. When we extend the sum over the entire phantom, which has large areas with homogeneous RSP, we find σ_{Rec} = 16.22 for L = 50 cm and σ_{Rec} = 15.42 for L = 30 cm. Selecting a 20 pixel × 20 pixel area around the white spot in the bottom center of Fig. 3, where the reconstruction accuracy depends on the spatial resolution, we find a much larger relative difference with σ_{Rec} = 0.53 for L = 50 cm and σ_{Rec} = 0.31 for L = 30 cm. Thus we set the distance L to the minimum distance permitting free rotation of the phantom, L =30 cm.

The depth of the energy detector is 30 cm of water equivalent thickness (WET), sufficient to stop 200 MeV protons.

3 TRACKER DESIGN AND R&D

The tracker has to measure the proton path with sufficient precision to allow the reconstruction of the MLP with sub-mm accuracy within the phantom. The sensors need to be fast, thin to limit MCS, and have fine pitch.

3.1 Silicon Sensors

Silicon strip sensors are an attractive choice since they have low noise at good efficiency, an important factor in a sparse system with no redundant space points. We will use single-sided silicon strip detectors (SSD) developed for the Fermi mission manufactured by Hamamatsu Photonics [10], with sensors with horizontal and vertical strips mounted back-to-back on printed circuit boards. In order to cover the active area, the sensors with 228 μm pitch from 6” wafers will be tiled as shown in Fig. 4. SSDs with vertical strips are read out individually, while those with horizontal strips are bonded together in pairs and read out at the end.

3.2 Slim Edges

One issue is that the wafer sizes are limited to 6” and that the active area of the sensors is surrounded by a 1 mm wide dead edge area, which prevents seamless tiling. In the prototype described in Ref. [5] the sensors were overlapped by 5 mm to have 100% coverage, which led to artifacts in the reconstructed images, when not taken into account properly. To avoid having to correct for this variation in effective sensor thickness, we are developing “slim edges” on Si sensors which will allow tiling without overlap and minimal dead area [11]. This is done in collaboration with the US Naval Research Lab (NRL). Slim edges can be fabricated on finished sensors in a “scribe-cleave-passivate” (SCP) treatment involving Laser + XeF_2 scribing, followed by cleaving and passivation of the edge with plasma-enhanced chemical-vapor-deposited (PECVD) nitride for n-type and atomic-layer-deposited ALD with alumina for p-type sensors. Details of the treatment are given in Ref. [11]. Pictures of a Fermi “Baby” detector [10] before treatment and with a slim edge without a guard ring, respectively, are shown in Fig. 5.

Figure 6 shows the total detector currents for the slim edge sensor of Fig. 5, which has an edge length of 3.5 cm, an area of 5.6 cm^2 and a thickness of 400 μm. At the depletion voltage of 100V, the currents are less than 100 nA when the guard ring is cut away as shown

in Fig. 5 and less than 10 nA when the cut is outside the guard ring (not shown). Individual strip currents before and after cutting are essentially unchanged. In addition, we have found that the charge collection on the strips next to the slim edge is unchanged when compared to before cleaving [12]. Up to now, about 50 test structures with edge length up to 10 cm have been treated successfully with distances down to 14 μm between active area and edge. For the existing Fermi sensors [10] with fairly large distances between implants (see Fig. 5), our process permits reducing the width of the dead edge area from 1 mm to less than 200 μm. The next step is extending the cleaving from the test structures to the full size sensors, for which industrial methods will be used.

3.3 Silicon Sensors Thickness

The thickness of the silicon sensors plays a role in tracking since the multiple scattering MCS reduces the accuracy with which proton tracks can be extrapolated into the phantom. From Fig. 2 one can understand that large MCS angles in the front detector ×2 and the back detector ×3 will go undetected and will distort the MLP determination. This is especially important for the protons traversing the phantom not at the center where the multiple scattering in the phantom is maximal and the extrapolation distance is smallest, but at larger lateral distances where the multiple scattering in the phantom is reduced and the extrapolation distance is larger. In that case, a more accurate determination of the entrance and exit location will improve the MLP calculation. Figure 7 shows a comparison between the MCS angle in one x-y plane (calculated according to Moliere's approximation) with the intrinsic resolution of the telescope due to the sensor pitch. This is done as a function of proton energy for 3 different thicknesses: 1600 μm for 4 SSD as in the overlap region of the present prototype, 800 μm for 2 SSD, both for sensors of 400 μm thickness, and 400 μm for 2 SSD of 200 μm thickness. Also indicated is the angular precision of the intra-telescopes distances D = 3, 5, 10 cm. At 200 MeV, the largest proton energy at the phantom entrance, the MCS angles of all plane thicknesses approach the intrinsic telescope precision. The angular precision with D = 3 cm exceeds or is comparable to the MCS angle for all sensor thicknesses, while the one with D=10 is much smaller than the MCS angle. Our choice of D=5 cm, driven by the compactness design goal, will have only a 10% reduction in overall angular resolution when compared to D=10 cm. At 80 MeV, the lowest proton energy at the phantom exit, the MCS angle exceeds the intrinsic telescope resolution. Therefore we consider using thinner sensors of 200 μm thickness (fabricated using the original Fermi mask set) in the first x-y plane of the back telescope (X3 in Fig. 2).

3.4 Data Flow in the Tracker

As mentioned before, increasing the data rate to exceed 2 MHz is the center part of the upgrade toward clinical application. Si sensors are intrinsically fast, so the solution is to design a readout ASIC faster than the one built for Fermi [13] and a distributed data acquisition (DAQ), employing local FPGAs for data collection, formatting and transmission. The concept of the DAQ is shown in Fig. 8. Twelve field programmable gate arrays (FPGAs) are needed to acquire the data from the 144 front-end ASICs, which read out the 32 single sided silicon strip detectors (SSDs). Twelve serial lines then carry the data from those FPGAs to the event builder, which sits on the DAQ computer PCI bus. The tracker data for a single proton will consist of about 350 bits. The high speed of the PCI bus allows complete events to flow into the computer's memory at the desired rate of at least a million protons per second. All digital signals are transmitted on low-voltage differential signal (LVDS) serial lines.

A SSD is read out by a 64 channel ASIC, which is being designed specifically for this high rate application. Each channel has a two-stage amplifier followed by a discriminator. The shaping time of the amplifier has been selected to match the time structure of the proton

beam of the Loma Linda University Center (LLUMC) synchrotron, which consists of "buckets" 100 ns apart within a much longer spill. Using a 200 ns peaking time of the amplifier, all tracker hits can be associated with a specific "bucket". The discriminator output is sampled by logic that looks for a rising edge. The resulting short pulses feed into a FIFO that holds the data long enough for a trigger decision to be made by the external logic. When the trigger is received, the data are transferred from the FIFO into one of four parallel event processors, which reduce the 64-channel data into a list of clusters, which is stored in one of four event buffers pending readout. A logical OR of all 64 channels is output asynchronously for use by the trigger logic, although we expect the main trigger to be done with the energy detector.

4 ENERGY/RANGE DETECTOR DESIGN AND R&D

For the required speed of the planned head scanner, the presently used CsI crystals are much too slow as a calorimeter material. We are planning to use polystyrene scintillator, which is very fast, but has the disadvantage to be less dense and thus requiring a longer energy detector.

4.1 Water Equivalent Path Length (WEPL)

The integrated S.P. measurement is equivalent to determining the Water Equivalent Path Length (WEPL) inside the phantom by subtracting the measured residual range from the range of the proton. This can be done by calibrating the detector with a set of degraders of known Water Equivalent Thickness WET (density and thickness), and extract the WEPL resolution as a function of the degrader thickness [14]. The different options to measure WEPL are shown schematically in Fig. 9. The energy/range detector is indicated by the segments S1 to Sn. A calorimeter consists of only one block (n=1), and a range counter has a large number of plates (n ≈ 100). A multi-stage detector is a hybrid between the two choices, consisting of a few blocks (n = 3 – 10).

4.2 Range Counter with direct SiPM Readout

The main challenge for the S.P. measurement in pCT is range/energy straggling. The straggling uncertainty is a function of depth, and for a stopping proton amounts to about 1% of the range. Since the energy loss in the phantom can't be measured directly, straggling in the phantom limits the accuracy of the energy/range measurement. A residual range detector [15] will always encounter the maximum range straggling, independent of the depth of the phantom, since the straggling material in phantom and range counter simply add. Geant4 simulations have shown that for 200 MeV protons, a polystyrene range counter with has almost constant resolution of close to 4 mm for plate thickness between 1 mm and 6 mm. We are pursuing a range counter with 4 mm plates, with direct readout using 3×3 mm^2 Silicon Photomultipliers (SiPM) and have good initial results using the HPK MCCP S10931-100P, shown on Fig 10. In a 200 MeV proton beam, the signal is 38 photo electrons (p.e.) when derived from the one p.e. signal, and 45 p.e. when derived from the width-to-peak ratio. As indicated in Fig. 10, the high photo electron yield permits a threshold of 5 p.e. without loss of efficiency and with an acceptable dark counting rate of less than 10 kHz.

4.3 Multi-Stage WEPL Detector

Because of the straggling limitation of the range detector we are pursuing also a hybrid multi-stage detector, combining coarse range with fine calorimeter measurements. For an initial test, we have implemented a 2-stage hybrid, called "Bulky", consisting of two polystyrene blocks of 10 cm × 10 cm cross section and 40 cm length read out at the end by 3" photo multiplier tubes (PMT). Obviously, this arrangement does not stop the direct 200 MeV proton beam, but can be used to understand systematic effects in a multi-stage

detector. To determine the WEPL, one converts the energy in the block in which the proton stops to WET and adds, if applicable, the WET of the block in front. Thus the energy which is measured is generally smaller than if measured in a calorimeter and thus has a smaller error.

A WEPL calibration of the 2-stage "Bulky" was performed in the 200 MeV proton beam of the LLUMC synchrotron, using degraders as described above. The initial results on its WEPL resolution as a function of degrader thickness WET are shown in Fig. 11, comparing "Bulky", the CsI calorimeter of our present prototype [5, 14], and a Monte Carlo simulation of a range counter with 4 mm polystyrene plates. The 2-stage hybrid performs better than the CsI calorimeter over the entire WET range, and its resolution is about 40% lower than the range detector. A 3-stage "Bulky" under construction would improve the data below WET = 50 mm, since it would be measured with the proton stopping in the 3rd stage, while it is now measured in the 2nd stage in transmission as dE/dx. An obvious drawback of this hybrid multi-stage detector with respect to a range detector is the need for continuous careful calibration, which would be a waste of proton beam time, and possible interference of magnetic fields in the gantry.

5 Conclusions

We are now arriving at a new phase in pCT with a dedicated detector development of a large-area scanner with data acquisition speed useful in clinical applications.

The most advanced R&D topics are slim edges for the silicon sensors of the tracking system, a hybrid multi-stage WEPL detector for the energy/range detector and a data acquisition system sustaining 2 MHz proton rate.

End-to-end simulation of the instrument has been essential for our understanding of the requirements and proper choice of the technical solution, yet many lessons were learned during operation of the existing prototype and reconstruction of the data.

The next crucial step will be technology transfer into a hospital environment and development of clinical testing protocols.

Acknowledgments

Ongoing and unwavering support by Prof. James M. Slater (LLUMC) made this project possible.

The project described was supported by Award Number R01EB013118 from the National Institute of Biomedical Imaging And Bioengineering (NIBIB). The content is solely the responsibility of the authors and does not necessarily represent the official views of the National Institute of Biomedical Imaging And Bioengineering or the National Institutes of Health.

References

1. Sadrozinski HF-W, et al. Toward Proton Computed Tomography. IEEE Trans. Nucl. Sci. 2004; 51:3.
2. Schulte R, et al. Conceptional design of a proton computed tomography system for applications in proton radiation therapy. IEEE Trans. Nucl. Sci. 2004; 51:866.
3. Williams DC. The most likely path of an energetic charged particle through a uniform medium. Phys. Med. Biol. 2004; 49:2899. [PubMed: 15285255]
4. Bruzzi M, et al. Prototype Tracking Studies for Proton CT. IEEE Trans. Nucl. Sci. 2007; 54:140.
5. Sadrozinski, HF-W., et al. Detector Development for pCT. Conference Record, 2011 IEEE NSS-MIC Conference; p. 4457

6. Penfold, S. PhD thesis Univ. of Wollongong. 2010. Image Reconstruction and Monte Carlo Simulations in the Development of Proton Computed Tomography for Applications in Proton Radiation Therapy.
7. Petterson, M., et al. Proton Radiography Studies for Proton CT. Conference Record, 2006 IEEE NSS-MIC Conference; p. 2276
8. Petterson, M. UC Santa Cruz Physics Department Senior Thesis. Jun 23. 2006 Resolution of a PMMA Phantom using 200 MeV Protons.
9. Herman, G. 2nd edition. Springer Verlag; N.Y.: 2009. Fundamentals of Computerized Tomography, Image Reconstruction from Projections; p. 56
10. Ohsugi T, et al. Design and properties of the GLAST flight silicon micro-strip sensors. Nucl. Instr. Meth. 2005; A 541:29.
11. Christophersen, M., et al. Alumina and Silicon Oxide/Nitride Sidewall Passivation for P- and N-Type Sensors. these Proceedings
12. Mori, R., et al. Charge collection measurements on slim-edge microstrip detectors. SCIPP 12/02, to be published in Journal of Instrumentation JINST
13. Johnson RP, et al. An amplifier-discriminator chip for the GLAST silicon-strip tracker. IEEE Trans. Nucl. Sci. 1998; 45:927.
14. Hurley RF, et al. Water-Equivalent Path Length Calibration of a Prototype Proton CT Scanner. 2011 to be published in Medical Physics.
15. Amaldi U, et al. Construction, test and operation of a proton range radiography system. Nucl. Instr. Meth. 2011; A629:337.

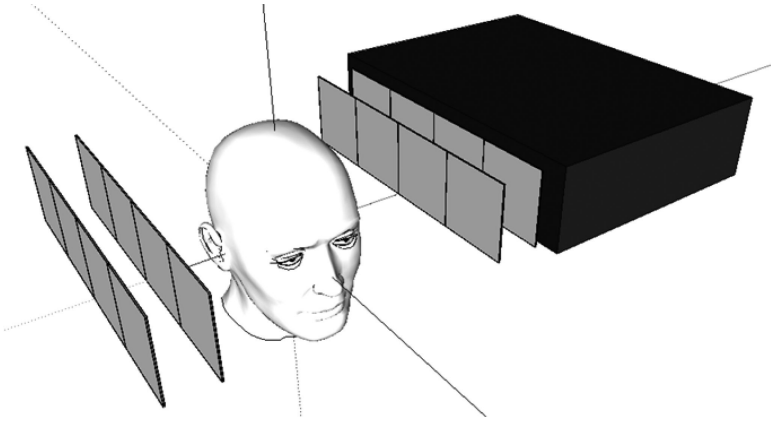

Fig. 1.
Layout of the pCT head scanner under construction. A proton entering from the left is first tracked in the entrance telescope of two x-y planes of silicon strip sensors, and after passing through the phantom/patient, in the similarly constructed exit telescope, before its residual energy/range is determined in the energy detector.

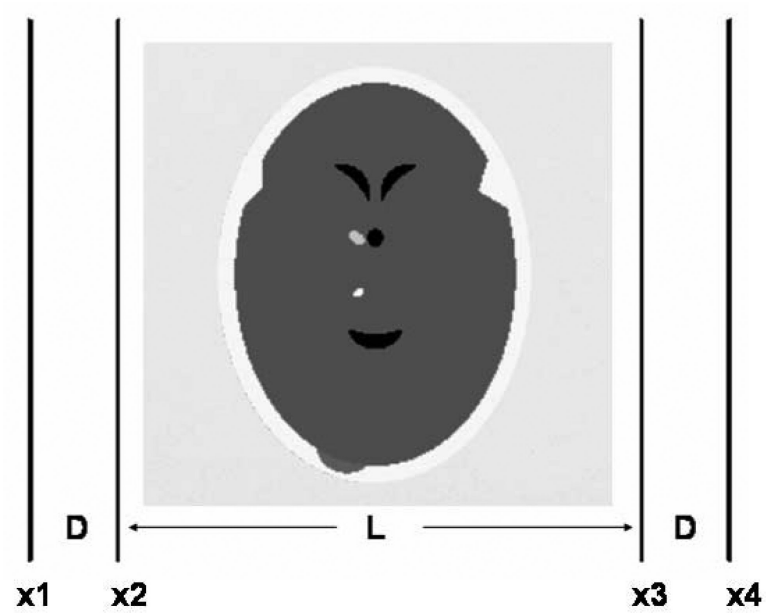

Fig. 2.
Critical tracker distances for simulations with a Herman head phantom [9]. L is the distance between front and back telescopes and D is the intra-telescope distance between the pair of x-y planes, taken to be the same in both front and back.

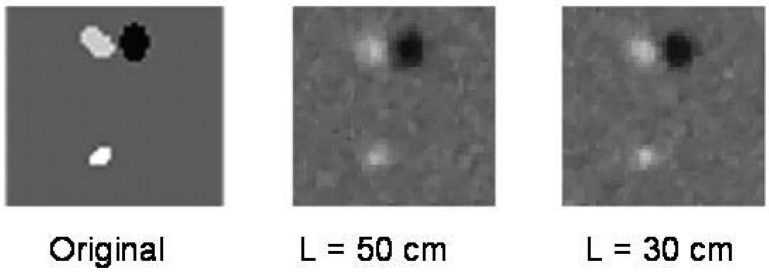

Fig. 3.
Original and pCT reconstruction of a Herman head detail [9] simulated with two distances between front and back telescope: L= 50 and 30 cm.

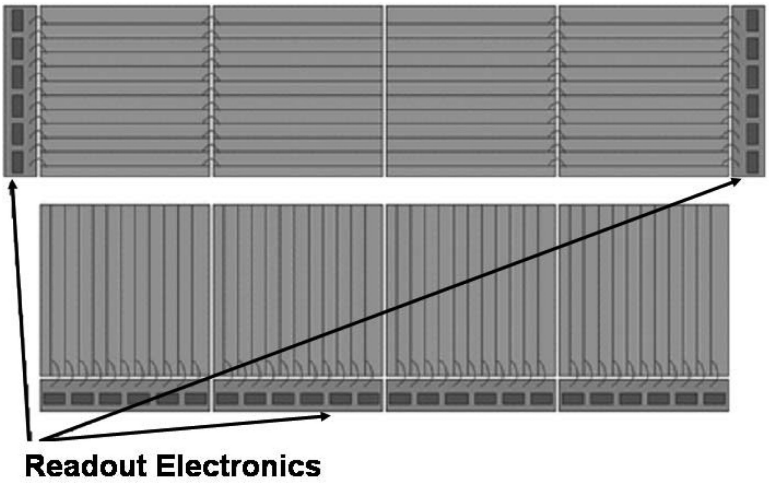

Fig. 4.

Layout of one x-y tracking planes of 6” silicon strip sensors, showing the two back-to-back sides separately, indicating the location of wire bonds and readout electronics. Pairs of sensors with horizontal strips are wire bonded together and read out at the ends.

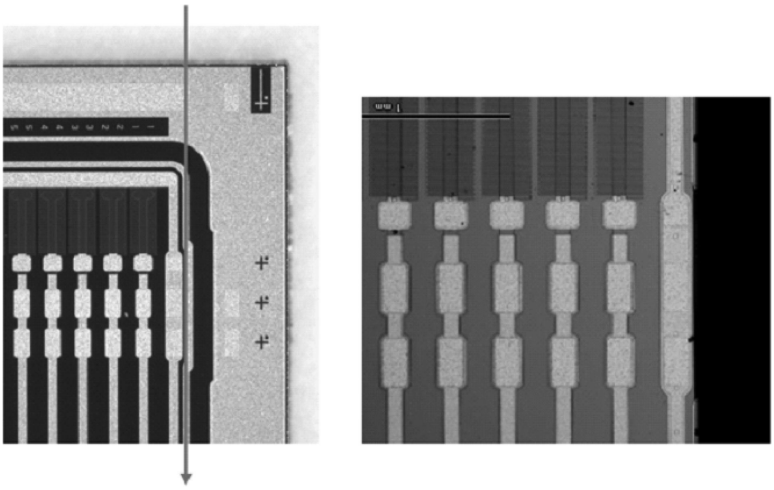

Fig. 5.
Generating a “slim” edge of less than 250 μm on a Fermi p-on-n “Baby” sensor [10]. The corner of the untreated sensor is shown on the left, with the planned cut between bias line and guard ring indicated by the vertical line. The SCP treated sensor is shown on the right, with the strips and the bias ring visible, but no guard ring. The strip pitch is 228 μm.

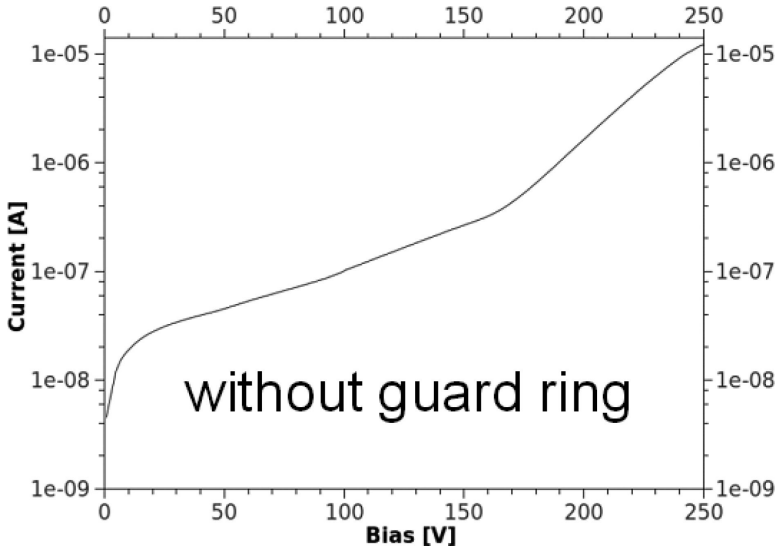

Fig. 6.
The I-V curve of a Fermi “Baby” after SCP treatment cleaving away the guard ring shows a leakage current of less than 100 nA at the operating voltage of 100 V.

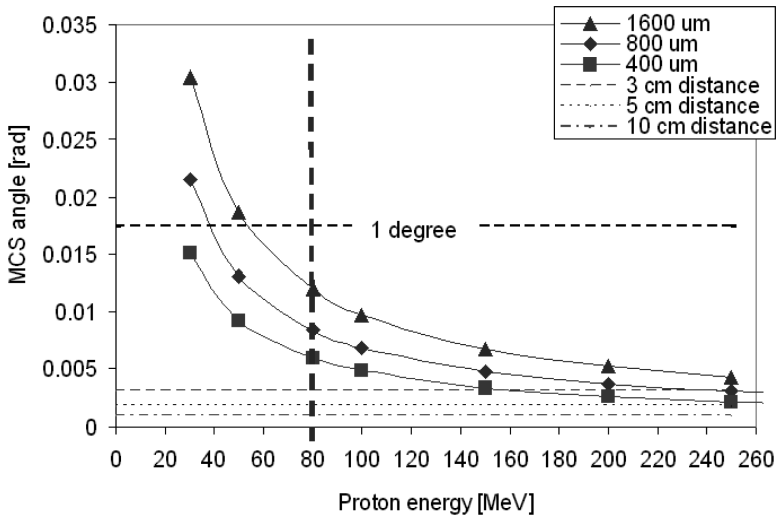

Fig. 7.

MCS angle vs. proton energy, for three thicknesses' of one x-y silicon plane. The minimum energy at the phantom exit is 80 MeV. Also shown are the angular precision of the silicon telescopes for three intra-telescope distances D. A typical MCS angle of the phantom is 2-4 degrees.

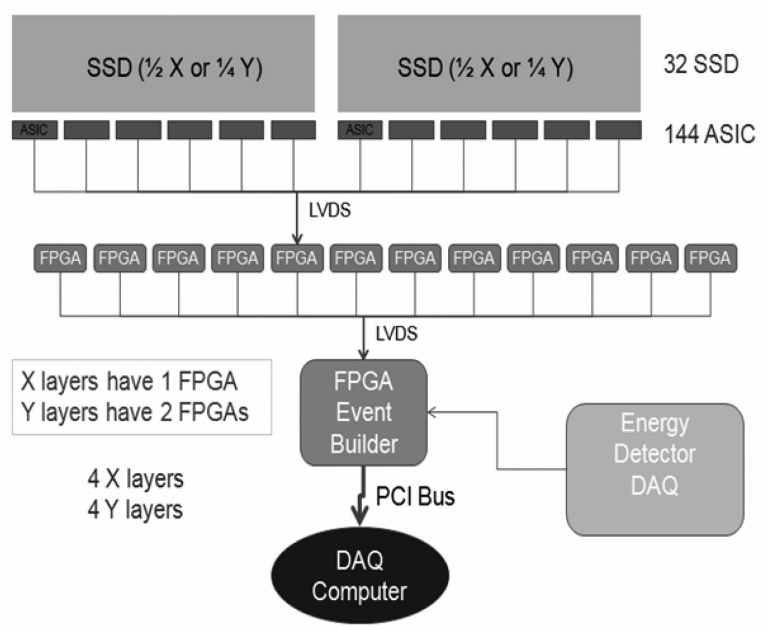

Fig. 8.
Data Flow block diagram, showing the distributed FPGAs within the DAQ.

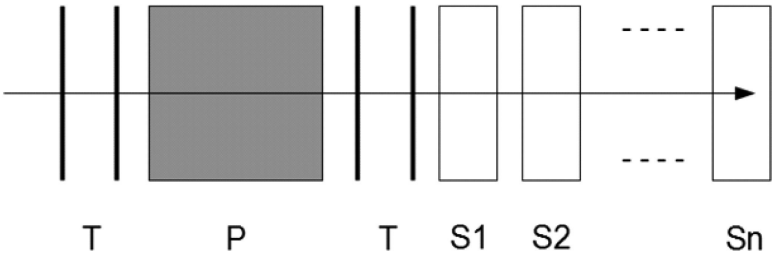

Fig. 9.
Schematic of the energy/range detector: n=1: calorimeter, n≈100: range counter, n=few: multi-stage detector (T = tracker telescopes, P =phantom).

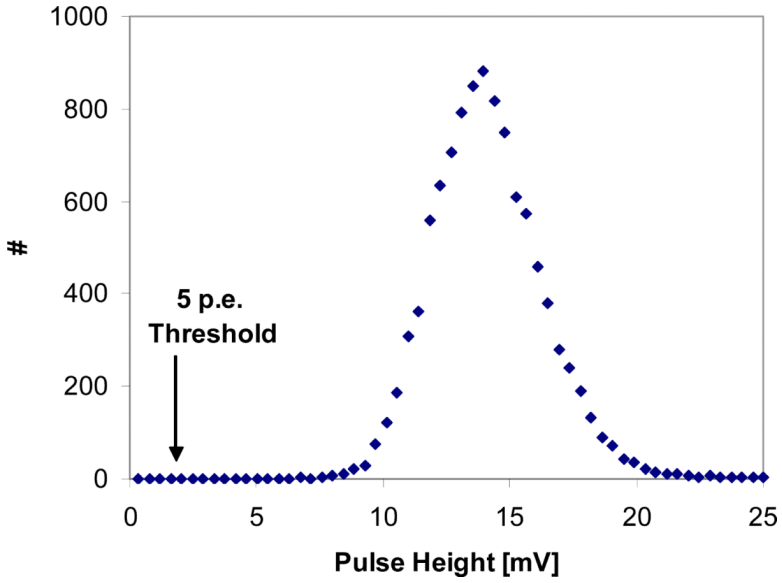

Fig. 10.

Measured pulse height signal of a 4.3 mm thick polystyrene plate with direct SiPM readout in a 200 MeV proton beam. The width of the distribution indicates a photo-electron yield of 45.

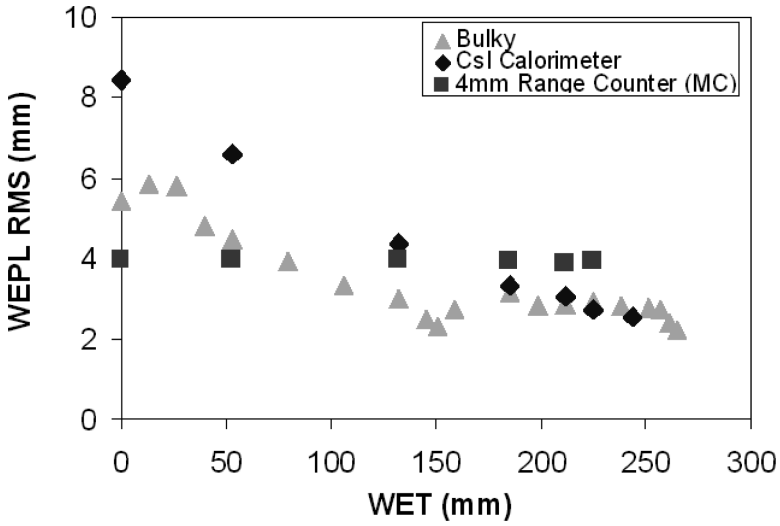

Fig. 11.
Comparison of the measured WEPL resolution for a CsI calorimeter [5, 14] and a 2-stage "Bulky" detector and the simulated WEPL RMS of a range counter with 4 mm polystyrene plates. The "Bulky" resolution is expected to improve below WET = 50 mm for a 3-stage detector.